Ultracompact photonic crystal polarization beam splitter based on multimode interference

Ming-Feng Lu,[1,2,*] Shan-Mei Liao,[1] and Yang-Tung Huang[1,3]

[1]Department of Electronics Engineering and Institute of Electronics, National Chiao Tung University, 1001 Da Hsueh Road, Hsinchu 30010, Taiwan

[2]Department of Electronic Engineering, Minghsin University of Science and Technology, 1 Hsin Hsin Road, Hsinfeng, Hsinchu 304, Taiwan

[3]Department of Biological Science and Technology, National Chiao Tung University, 1001 Da Hsueh Road, Hsinchu 30010, Taiwan

*Corresponding author: mflu@must.edu.tw

Received 21 September 2009; revised 6 January 2010; accepted 12 January 2010; posted 13 January 2010 (Doc. ID 117443); published 28 January 2010

We propose a theoretical design for a compact photonic crystal (PC) polarization beam splitter (PBS) based on the multimode interference (MMI) effect. The size of a conventional MMI device designed by the self-imaging principle is not compact enough; therefore, we design a compact PC PBS based on the difference of the interference effect between TE and TM modes. Within the MMI coupler, the dependence of interference of modes on propagation distance is weak for a TE wave and strong for a TM wave; as a result, the length of the MMI section can be only seven lattice constants. Simulation results show that the insertion losses are 0.32 and 0.89 dB, and the extinction ratios are 14.4 and 17.5 dB for Port 1 (TE mode) and Port 2 (TM mode), respectively.

OCIS codes: 230.5298, 230.1360, 130.2790, 130.5296, 230.5440.

1. Introduction

Optoelectronic devices with photonic crystals (PCs) have attracted extensive interest in recent years. PCs are artificial materials with periodically modulated refractive indices that exhibit photonic bandgaps (PBGs) [1,2]. The propagation of light with frequency within PBGs is forbidden. While introducing line defects into PC structures, PC waveguides are formed and provide a powerful way to manipulate the flow of electromagnetic waves. PC devices based on the multimode interference (MMI) effect can be much smaller than conventional MMI devices due to the large dispersion in PC structures [3]. MMI phenomena exist in multimode devices. A field profile can be reproduced in single or multiple images at regular intervals along the path of propagation based on the self-imaging principle [4]. The MMI effect can be used in applications of optical power splitters/combiners, switches, wavelength demultiplexers, Mach–Zehnder interferometers, couplers, etc. [5–8]. Conventional MMI devices have features such as simple structure, low polarization dependence, low loss, and large optical bandwidth. In the area of PCs, more and more researchers have focused on this topic. PC power splitters, filters, switches, and couplers based on the MMI effect and self-imaging principle have been proposed [9–13].

Polarization beam splitters (PBSs) split an unpolarized beam into two beams with orthogonal polarizations. Conventional polarizers can be designed by reflection of the Brewster's angle, birefringent crystals, or thin-film technology [14]. PBSs are important components for integrated optoelectronic circuits and can also be realized on PC structures. Design, fabrication, and measurement of a PC polarization splitter made by the autocloning technology have been reported [15,16]. A two-dimensional (2D) grat-

0003-6935/10/040724-08$15.00/0

ing coupler was proposed as a polarization splitter [17]. The microwave-scale PBS has been experimentally demonstrated on 2D PCs [18]. A compact PBS based on a PC directional coupler with a triangular lattice of airholes has been designed and simulated [19]. Its polarization separation functionality is enabled by two different guiding mechanisms: the PBG effect for transverse-electric (TE) light and an index-like effect for transverse-magnetic (TM) light, which makes the two channels of the directional coupler decoupled for TE and tightly coupled for TM light. A PBS and a nonpolarizing beam splitter (NPBS) based on a PC directional coupler that consists of a honeycomb lattice of dielectric pillars in air has been presented [20]. A resonant-coupling-type PBS based on a PC structure with absolute PBG was proposed [21]. Theoretical and experimental results of PC PBSs that exhibit a large reflection coefficient for TE and a high transmission coefficient for TM polarization have been presented [22,23]. Besides prism, grating, directional coupler, and cavity, a PBS can also be realized by the negative refractive property of PC structures. A PBS where TM polarization is refracted in the positive direction while the TE component is negatively refracted has been proposed [24].

The length of a conventional PBS designed by the MMI effect could be too long, because conventional MMI waveguides are insensitive to polarizations of waves. Maybe that is why, to our knowledge, no one has yet designed a PC PBS using the MMI effect. Dispersions of two polarization states in a PC structure are different; therefore, a PC PBS based on the MMI effect should be much smaller than a conventional one. In this study, we will present that the device size of a PC PBS designed by the self-imaging principle is not compact enough. Thus, a PC PBS based on the difference of the interference effect between the TE and TM modes is proposed. Because the band diagram of a dielectric-rod PC structure is simple, to clarify the design concept, we will investigate the MMI phenomenon on a dielectric-rod PC structure. First, the parameters of guided modes are extracted from the band diagrams calculated by the plane wave expansion (PWE) method. Modal propagation analysis (MPA), as used in conventional multimode devices, is used to predict the image positions [25]. Then the steady-state field distribution is simulated by the 2D finite-different time-domain (FDTD) method to have the actual image positions. Through these theoretical procedures, an ultracompact PC PBS based on the MMI effect can be designed. The length of the MMI region can be only seven lattice constants.

In the following sections, the self-imaging phenomena in PC multimode waveguides will be investigated. The performance of a PBS with a dielectric-rod PC structure designed by the self-imaging principle will be discussed. Next, a compact PC PBS based on the difference of the interference effect between TE and TM modes will be proposed. Finally, the performance of this compact device will be evaluated.

2. Design of a Multimode-Interference-Based PC PBS by Using the Self-Imaging Principle

The operation of conventional MMI devices is based on the self-imaging principle. In conventional optical waveguides, approaches that make use of ray optics [26], the beam propagation method, or the hybrid method [27,28] are used to predict the image positions within multimode devices. Because the light confinement in a PC waveguide is due to the PBG, not the total internal reflection, self-imaging phenomena in PC waveguides are not the same as those in conventional waveguides. Therefore, the approximated equations and the rules for designing conventional MMI devices cannot be directly applied to those cases in PC waveguides. The mode propagation analysis (MPA) method is the most useful tool for describing the self-imaging phenomena in multimode waveguides [25]. Here we use the MPA method to analyze the imaging lengths in PCs.

Assuming that the input wave is continuous and its spatial spectrum of field is narrow enough not to excite unguided modes, the total input field $\Psi(y,0)$ at $z=0$ in a multimode region can be decomposed into the guided modes and expressed as

$$\Psi(y,0)=\sum_{n=0}^{p-1}c_n\varphi_n(y), \tag{1}$$

where $\varphi_n(y)$ is the modal field distribution, c_n is the field excitation coefficient, p is the number of modes, and the subscript n denotes the order of modes $(n=0,1,2,\ldots,p-1)$. The field excitation coefficient c_n can be estimated using overlap integrals based on the field-orthogonality relation as

$$c_n=\frac{\int\Psi(y,0)\varphi_n(y)\mathrm{d}y}{\int\varphi_n^2(y)\mathrm{d}y}. \tag{2}$$

Assuming the time dependence implicit hereafter and taking the phase of the fundamental mode as a common factor, the field profile at a distance z can then be written as a superposition of all the guided mode field distributions:

$$\Psi(y,z)=\sum_{n=0}^{p-1}c_n\varphi_n(y)\exp[j(\beta_0-\beta_n)z]. \tag{3}$$

The profile of $\Psi(y,z)$ and the types of images formed are determined by the modal excitation coefficient c_n and by the properties of the mode phase factor $\exp[j(\beta_0-\beta_n)z]$, where β_0 and β_n are the propagation constants of the fundamental mode and the nth mode.

Then, the length of direct images, L_d, satisfies

$$(\beta_0-\beta_n)L_d=2p_n\pi,\quad \text{with}\, p_n=1,2,3,\ldots, \tag{4}$$

and we obtain

$$\Psi(y, L_d) = \Psi(y, 0). \quad (5)$$

This condition means that the phase changes of all modes after propagating L_d must differ by integer multiples of 2π, and all guided modes interfere with the same relative phases as those at $z = 0$. Thus, the image at a distance L_d is a direct replica of the input field.

On the other hand, the length of mirror images, L_m, satisfies

$$(\beta_0 - \beta_n)L_m = 2q_n\pi \quad \text{for even modes, and}$$
$$(\beta_0 - \beta_n)L_m = (2q_n - 1)\pi \quad \text{for odd modes, with}$$
$$q_n = 1, 2, 3, \ldots. \quad (6)$$

This condition means that the even modes are in phase and the odd modes are out of phase after propagating the length of mirror images. In the case of structural symmetry with respect to the plane $y = 0$, we obtain

$$\Psi(-y, L_m) = \Psi(y, 0). \quad (7)$$

Thus, the image at a distance L_m is a mirrored replica of the input field.

An MMI coupler can separate two waves if one wave is a direct image at one output of the coupler and another wave is a mirrored image at another output. This design concept is widely used in conventional beam splitters based on MMI. In the following, a PC PBS that is based on the self-imaging principle and can separate TE and TM waves will be designed [29]. In this study, the TE polarization indicates that the electric field is perpendicular to the normal of the lattice plane, which follows the convention used in a photonic crystal.

To design a PBS, the first requirement is that both TE and TM light can propagate with low loss in a PC waveguide. There is no TE gap while the refractive index $n < 3.5$ for a square lattice of dielectric rods in air. Therefore, to have a PC structure with a joint bandgap, the PC structure we studied is a square lattice of dielectric rods with refractive index 4.1. Germanium with a refractive index of 4.1 is a promising material that is widely used in advanced semiconductor processes. That results in the largest joint bandgap at $r = 0.38a$, where r is the radius of the dielectric rods and a is the lattice constant of the PC. The frequency range of the complete bandgap is from 0.455 to 0.475 (a/λ), where λ is the wavelength in free space. However, the lower edge of the bandgap at X point is extended to 0.44 (a/λ).

The schematic structure of the PC PBS to be designed is shown in Fig. 1. It is basically a 1×2 MMI coupler and has one input access port and two output access ports, Port 1 and Port 2. A single-line-defect PC waveguide that is formed by removing one row of dielectric rods along the Γ–X direction in the square lattice acts as the access waveguide and is denoted by W1. Wn stands for a PC waveguide with n rows of dielectric rods removed. The high transmission frequency of this W1 PC waveguide is around 0.444 (a/λ) for TE and TM waves, so 0.444 (a/λ) is chosen as the operating frequency.

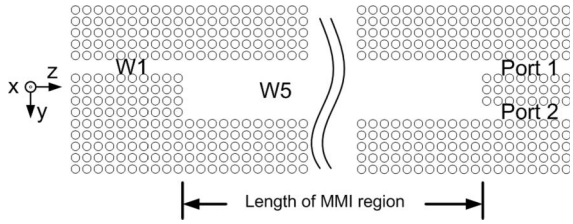

Fig. 1. Schematic structure of a PC PBS based on the MMI effect. The 1×2 MMI coupler has one input and two output access ports. W1 PC waveguides act as the access waveguides. A W5 PC waveguide acts as the multimode interference region and its section length is to be designed.

The W5 PC waveguide acts as the multimode interference region and its length is to be designed. The imaging property of a waveguide is linked to the characteristic of its spectrum of propagation constants. The TE projected band diagram of the W5 PC waveguide simulated by the PWE method is shown in Fig. 2(a). It can be seen that this multimode PC waveguide supports four modes for a TE wave at an operating frequency of 0.444 (a/λ). These modes in the wide defect region lead to the operation of

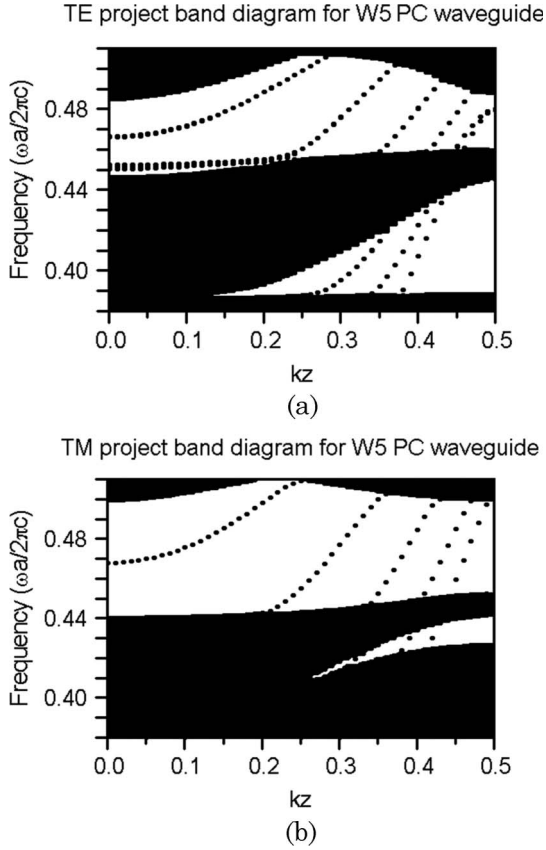

Fig. 2. (a) TE and (b) TM projected band diagram of the W5 PC waveguide.

Table 1. Parameters Used to Calculate the Locations of Images of the W5 Photonic Crystal Waveguide for a Transverse-Electric Wave at 0.444 (a/λ)

Mode	Parity	$\beta_n(2\pi/a)$	$L_C = \pi/(\beta_0 - \beta_n)$	First Mirror Image	First Direct Image
0	even	0.441	-	-	-
1	odd	0.429	$43a$	$L_C \times 1 = 43a$	$L_C \times 2 = 86a$
2	even	0.395	$11a$	$L_C \times 4 = 44a$	$L_C \times 8 = 88a$
3	odd	0.312	$3.9a$	$L_C \times 11 = 43a$	$L_C \times 22 = 86a$

MMI. The parameters about these modes, including propagation constants and the symmetry property of modal field patterns, are listed in Table 1. The coupling length between the fundamental mode and the nth mode is defined as $L_C = \pi/(\beta_0 - \beta_n)$. It can be calculated that the coupling length between the fundamental mode and the first mode is $44a$ and self-imaging exists if all coupling lengths are very nearly the integer multiples of this fundamental difference, as described by Eqs. (4)–(7). The lengths of direct images L_d and mirror images L_m can be calculated from these parameters by Eqs. (4) and (6), respectively. Consequently, the first mirror image and the direct image are estimated at $44a$ and $88a$ in this multimode region.

The TM projected band diagram of this W5 PC waveguide calculated by the PWE method is illustrated in Fig. 2(b). From these dispersion curves, it can be seen that this PC multimode waveguide supports four defect modes for a TM wave at an operating frequency of 0.444 (a/λ). The parameters about these modes are listed in Table 2. It is estimated that there is a mirror image at $88a$ in the multimode region for a TM wave. If the length of the W5 PC waveguide is designed as $88a$, the TE wave will be a direct image at Port 1 and the TM wave will be a mirror image at Port 2. Consequently, we can use the difference of imaging lengths between two polarizations to design a PBS that can separate TE and TM waves.

The steady-state electric field distributions of this PC PBS simulated by the 2D FDTD method for TE and TM waves are shown in Figs. 3(a) and 3(b), respectively. The TE wave will be routed to the lower output port (Port 2) and the TM wave to the upper output port (Port 1). The transmissions, bending losses, and extinction ratios for the two output ports are listed in Table 3. Simulation results show that the extinction ratios are 12.8 dB for Port 1 and 9.2 dB for Port 2. The extinction ratio for one output port is defined as the power of the desired field to that of the undesired field and is expressed as $10\log(P_{\mathrm{TE(TM)}}/P_{\mathrm{TM(TE)}})$. The insertion losses are 0.79 dB for Port 1 and 0.30 dB for Port 2. The insertion loss is the attenuation expressed in decibels for a particular path through the component and is defined as $10\log(P_{\mathrm{port1(2)}}/P_{\mathrm{input}})$. To avoid the coupling between these two output waveguides, a 90° bend is added to the upper output waveguide and the insertion loss of Port 2 includes the bending loss 0.27 dB. Compared to other PC PBSs, the size of this PC PBS designed by the self-imaging principle is not compact enough and we will design a more compact one with a different design consideration.

Table 2. Parameters Used to Calculate the Locations of Images of the W5 Photonic Crystal Waveguide for a Transverse-Magnetic Wave at 0.444 (a/λ)

Mode	Parity	$\beta_n(2\pi/a)$	$L_C = \pi/(\beta_0 - \beta_n)$	First Mirror Image
0	even	0.431	-	-
1	odd	0.402	$17.3a$	$L_C \times 5 = 87a$
2	even	0.341	$5.6a$	$L_C \times 16 = 89a$
3	odd	0.243	$2.6a$	$L_C \times 34 = 88a$

3. Design of a Compact PC PBS by Difference of Interference between Two Polarizations

The imaging distance for TE polarization is found to be longer than that for TM polarization in conventional MMI devices. This phenomenon may be interpreted as a manifestation of the Goos–Hähnchen effect [25]. In a PC structure, it is also found that the imaging lengths for a TE wave and for a TM wave are different. This phenomenon can be interpreted by anisotropy of a photonic band structure [15]. It can be seen that there are many high-intensity points, except in the self-images in Fig. 3(b). In the following, a compact PC PBS will be designed using the high-intensity point instead of the self-imaging principle.

To verify the interference difference between two polarizations, we observe the steady-state field distribution in an open-ended W5 PC waveguide, as shown in Fig. 4, by using the 2D FDTD method. According to the central line ($y = 0$) of the open-ended W5 PC waveguide, the upper-half portion is called Channel 1 and the lower half is called Channel 2. The optical powers within Channel 1 and Channel 2 are measured by Monitors A and B, respectively. Transmissions of a TE wave measured by Monitor A (solid curve) and Monitor B (dashed curve) under different positions within the W5 PC waveguide are shown in Fig. 5. The transmission is defined as the ratio of the measured power to the input power. It can be seen that the first peaks of transmission along

Table 3. Transmissions, Bending Losses, and Extinction Ratios of the PC PBS

	Transmission			
	TE	TM	Bending Loss	Extinction Ratio
Port 1	4.7%	88.8%	0.27 dB	12.8 dB
Port 2	93.3%	11.2%	None	9.2 dB

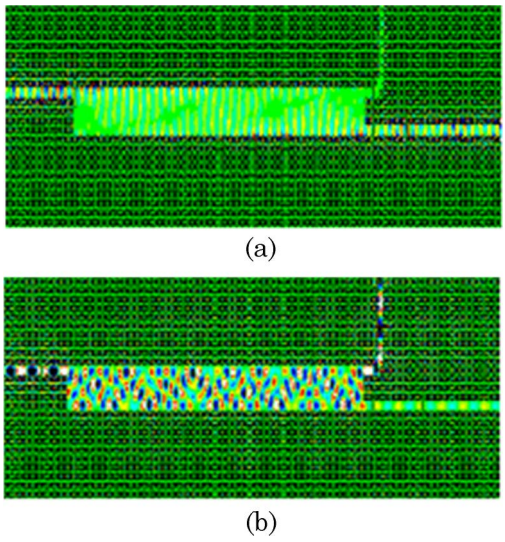

Fig. 3. (Color online) Steady-state electric field distributions of the PC PBS designed by the self-imaging principle for (a) a TE, and (b) a TM wave.

Channel 2 and Channel 1 happen at $44a$ and $88a$, respectively. That is consistent to the imaging lengths calculated from Table 2.

On the other hand, transmissions of a TM wave measured by Monitor A (solid curve) and Monitor B (dashed curve) under different positions within the W5 PC waveguide are shown in Fig. 6. Compared with the case of a TE wave, the field distribution due to the interference effect for a TM wave is strongly dependent on the propagation distance in this PC structure. It can be seen that peak values happen alternatively along Channel 1 and Channel 2 with a period of about $9.8a$, and the first peak of the transmission along Channel 2 appears at $6a$.

Next we will use the PWE method to reveal why there is a transmission peak at $6a$ along Channel 2 for a TM wave. The normalized field profiles of the W1 and W5 PC waveguides for the TM mode are shown in Figs. 7(a) and 7(b), respectively. These field profiles are taken from the central plane (x–y plane at $z = 0$) of the supercell calculated by the PWE method. Though the field profiles are not uniform along the z axis within a supercell, they can be approximately represented by the field profile taken from the central plane due to the strong confinement of light within a PBG. The normalized field excitation

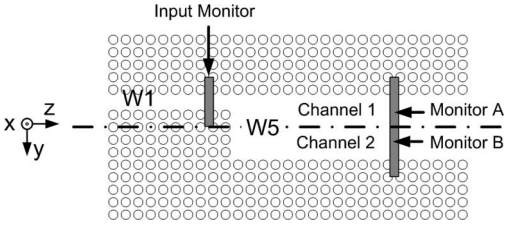

Fig. 4. Open-ended W5 PC waveguide to be studied. The optical powers within the upper- (Channel 1) and lower- (Channel 2) half portions of the open-ended W5 PC waveguide are measured by Monitors A and B, respectively.

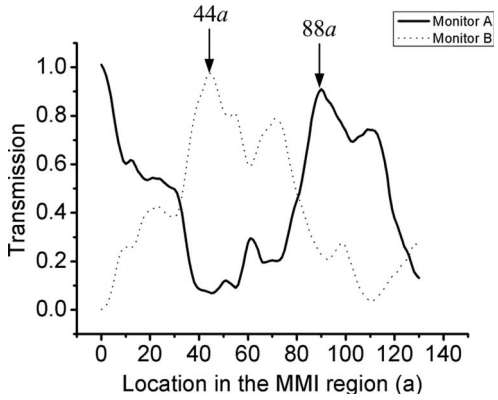

Fig. 5. Transmissions of a TE wave measured by Monitor A (solid curve) and Monitor B (dashed curve) under different positions within the W5 PC waveguide. The first peaks of transmission along Channel 2 and Channel 1 happen at about $44a$ and $88a$, respectively.

coefficients calculated from these field profiles by Eq. (2) are 0.2452, −0.4797, −0.5740, and 0.6167.

According to Eq. (1), the field profile at a distance of z within the W5 PC waveguide can be written as

$$\begin{aligned}\Psi(y,z) = \sum_{n=0}^{3} c_n \varphi_n(y) \exp[j\beta_n z] &= 0.2452 \times \varphi_0 \\ &\times \exp[j2\pi \times 0.431z] - 0.4797 \times \varphi_1 \\ &\times \exp[j2\pi \times 0.402z] - 0.5740 \times \varphi_2 \\ &\times \exp[j2\pi \times 0.341z] + 0.6167 \times \varphi_3 \\ &\times \exp[j2\pi \times 0.213z]. \end{aligned} \tag{8}$$

The power profile of these modes within the W5 PC waveguide calculated by Eq. (8) is shown in Fig. 8(a). The intensity distributions counterchange between Channel 1 and Channel 2, and strongly depend on the propagation distance. High intensity happens when these fields are constructive; therefore, the first peak of transmission along Channel 2 for a TM wave appears at $z = 6a$. The real part (dashed curve) and imaginary part (dotted curve) of the field superposition of all modes along z axis at $y = 2a$ are

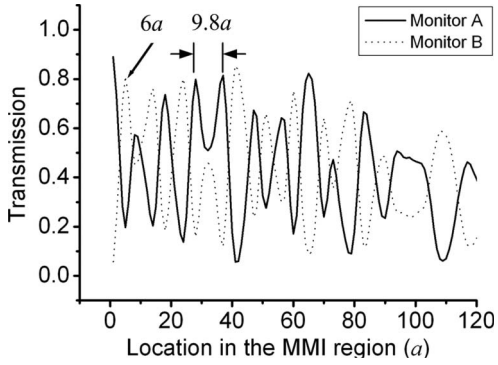

Fig. 6. Transmissions of TM wave measured by Monitor A (solid curve) and Monitor B (dashed curve) under different positions within the W5 PC waveguide.

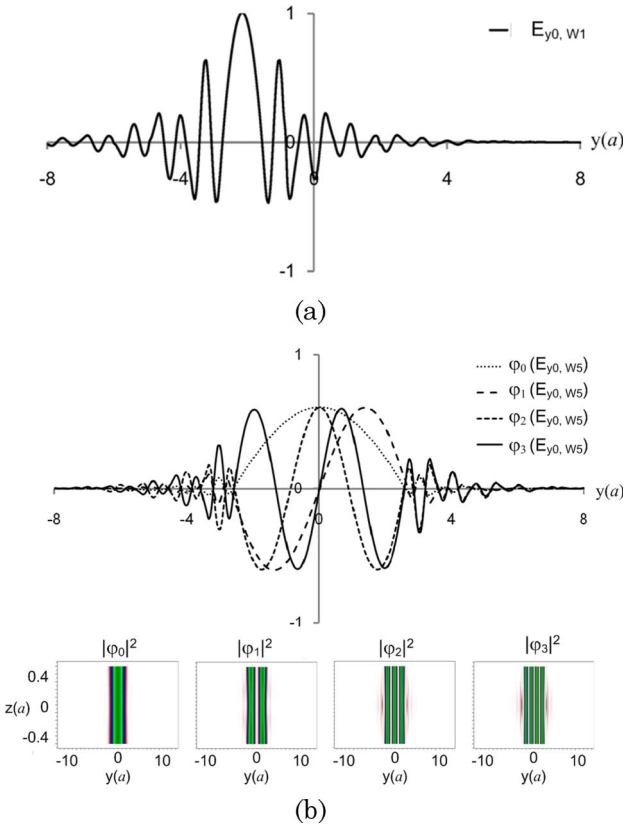

Fig. 7. (Color online) Normalized field profiles of the (a) W1 and (b) W5 PC waveguides.

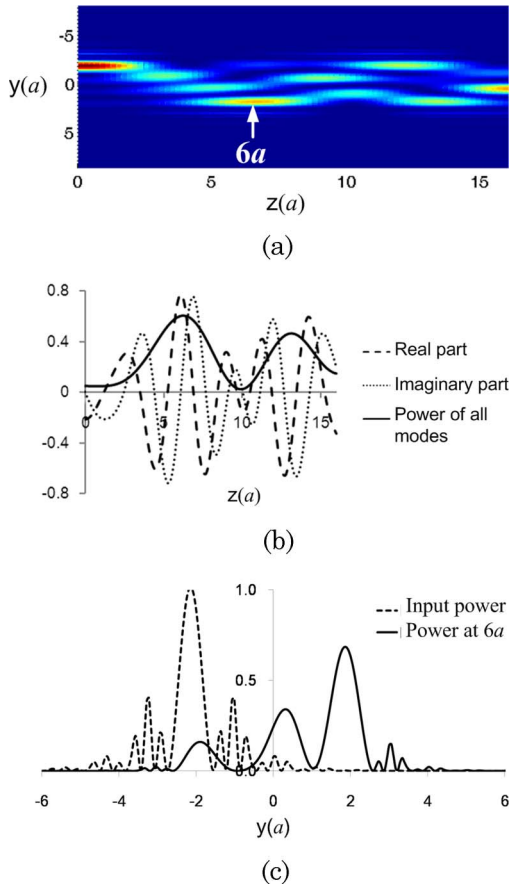

Fig. 8. (Color online) (a) Power profile of all TM modes within the W5 PC waveguide. (b) Field superposition of all modes along the z axis at $y = 2a$. (c) Power profile of a TM wave at $z = 6a$.

shown in Fig. 8(b). These fields form a beat wave with a period of $9.8a$ (solid curve), and the first peak happens at $z = 6a$. That is consistent to the dashed curve in Fig. 6. Image quality is an important factor while designing by the self-imaging principle. To reveal the image quality, the power profile of all modes at $z = 6a$ is shown in Fig. 8(c). Although the profile of a TM wave at $z = 6a$ is not a true mirror image of the input wave, the power within Channel 2 of the W5 PC waveguide is about 84% for this open-ended structure.

It has been shown that the interference effect within the MMI coupler for a TM wave is more sensitive to the propagation distance than that for a TE wave. We can use this different behavior between TE and TM polarizations to design a compact PBS that can separate these two waves. The transmissions of a TE wave measured by Monitor A (solid curve) along Channel 1 in Fig. 5 and a TM wave measured by Monitor B (dashed curve) along Channel 2 in Fig. 6 are redrawn in Fig. 9. It can be seen that both transmissions along Channel 1 for a TE wave and Channel 2 for a TM wave are high at $6a$. Therefore, the ultracompact PC PBS we designed is shown in Fig. 10. The length of the MMI section is only seven lattice constants. To avoid the coupling between two output waveguides, a 90° bend is added to the lower output waveguide. The TM wave will be routed to the lower output port (Port 2) after a propagation distance of the first peak along Channel 2. On the other hand, the TE wave will travel directly to the upper output port (Port 1) because its interference effect is weakly dependent on the propagation distance. The MMI coupler can separate two waves because it is a bar coupler for one wave and a cross coupler for another wave.

The steady-state electric field distributions of this PC PBS for TE and TM waves are shown in Figs. 11(a)

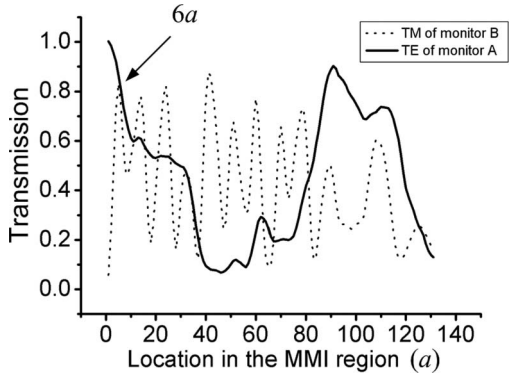

Fig. 9. Transmissions of TM wave measured by Monitor B (dashed curve) in Fig. 6 and TE wave measured by Monitor A (solid curve) in Fig. 5 under different positions within the W5 PC waveguide. It can be seen that both transmissions at Channel 1 for TE wave and at Channel 2 for TM wave are high at $6a$.

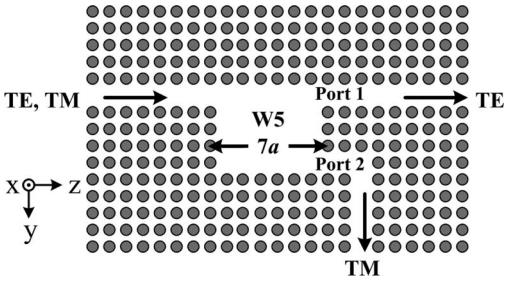

Fig. 10. Structure of the ultracompact PC PBS. The length of the MMI region is only 7*a*. The TE wave is routed to the upper output port (Port 1) and the TM wave to the lower output port (Port 2).

and 11(b), respectively. It can be seen that the separation function of polarization beams works well. Transmissions, bending losses, and extinction ratios of this compact PC PBS are listed in Table 4. Simulation results show that the insertion losses are 0.32 and 0.89 dB, and the extinction ratios are 14.4 and 17.5 dB for Port 1 (TE mode) and Port 2 (TM mode), respectively. The insertion loss of Port 2 includes the bending loss 0.7 dB. Note that the transmission

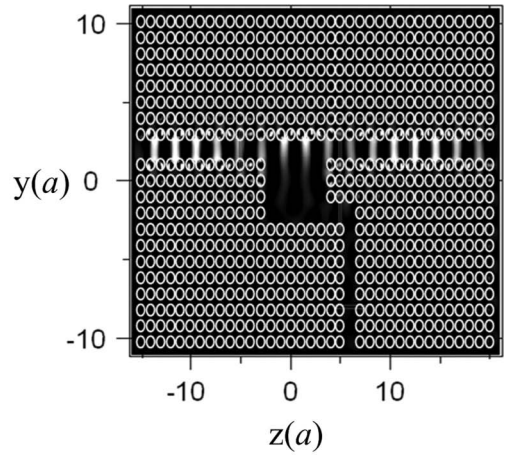

(a)

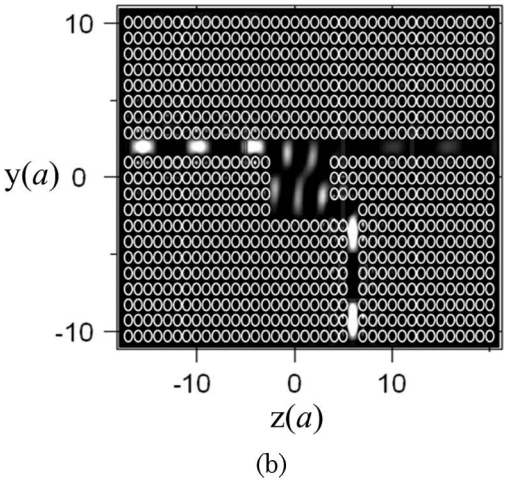

(b)

Fig. 11. Steady-state electric field distributions of the compact PC PBS for (a) TE and (b) TM waves.

Table 4. Transmissions, Bending Losses, and Extinction Ratios of the Compact PC PBS

	Transmission			
	TE	TM	Bending Loss	Extinction Ratio
Port 1	93.0%	3.4%	None	14.4 dB
Port 2	1.7%	95.8%	0.7 dB	17.5 dB

at 6*a* is about 84% for an open-ended W5 PC waveguide, as shown in Fig. 9, and improved to above 93% for this PC PBS due to the existence of output waveguides. Seven lattice constants is the optimal length of the MMI section in this study. The PC PBS based on a directional coupler has been reported with a length of 24.2 μm [19]. Insertion losses and extinction ratios are found to be around 0.8 dB and 18–20 dB in other studies [17]. Therefore, this proposed MMI-based PC PBS has a compact size and high extinction ratio.

4. Conclusion

The design method of a compact PC PBS based on the difference of the interference effect between TE and TM polarizations is presented. The MMI region is a bar coupler for a TE wave and is a cross coupler for a TM wave, and its length is only 7*a*. To our knowledge, this is the first study shows that a PC PBS can be designed by the MMI effect. Simulation results show that the insertion losses are 0.32 and 0.89 dB, and the extinction ratios are 14.4 and 17.5 dB for output Port 1 (TE mode) and output Port 2 (TM mode), respectively. Compared with conventional counterparts of millimeter scale and other PC devices designed by the self-imaging principle, this MMI-based PC PBS has advantages of compactness and low loss.

This work was supported in part by the National Science Council of Taiwan (NSCT) under grants NSC 97-2221-E-159-003 and NSC 97-2221-E-009-032.

References

1. E. Yablonovitch, "Inhibited spontaneous emission in solid-state physics and electronics," Phys. Rev. Lett. **58**, 2059–2062 (1987).
2. S. John, "Strong localization of photons in certain disordered dielectric superlattices," Phys. Rev. Lett. **58**, 2486–2489 (1987).
3. T. Liu, A. R. Zakharian, M. Fallahi, J. V. Moloney, and M. Mansuripur, "Multimode interference-based photonic crystal waveguide power splitter," J. Lightwave Technol. **22**, 2842–2846 (2004).
4. L. B. Soldano and E. C. M. Pennings, "Optical multi-mode interference devices based on self-imaging: principles and applications," J. Lightwave Technol. **13**, 615–627 (1995).
5. M. R. Paiam, C. F. Janz, R. I. MacDonald, and J. N. Broughton, "Compact planar 980/1550 nm wavelength multi/demultiplexer based on multimode interference," IEEE Photon. Technol. Lett. **7**, 1180–1182 (1995).
6. Z. Li, Z. Chen, and B. Li, "Optical pulse controlled all-optical logic gates in SiGe/Si multimode interference," Opt. Express **13**, 1033–1038 (2005).

7. T. Y. Tsai, Z. C. Lee, J. R. Chen, C. C. Chen, Y. C. Fang, and M. H. Cha, "A novel ultra compact two-mode-interference wavelength division multiplexer for 1.5 μm operation," IEEE J. Quantum Electron. **41**, 741–746 (2005).
8. X. Jia, S. Luo, and X. Cheng, "Design and optimization of novel ultra-compact SOI multimode interference optical switch," Opt. Commun. **281**, 1003–1007 (2008).
9. H. J. Kim, I. Park, B. H. O, S. G. Park, E. H. Lee, and S. G. Lee, "Self-imaging phenomena in multi-mode photonic crystal line-defect waveguides: application to wavelength de-multiplexing," Opt. Express **12**, 5625–5633 (2004).
10. Y. Zhang, Z. Li, and B. Li, "Multimode interference effect and self-imaging principle in two-dimensional silicon photonic crystal waveguides for terahertz waves," Opt. Express **14**, 2679–2689 (2006).
11. Z. Li, Y. Zhang, and B. Li, "Terahertz photonic crystal switch in silicon based on self-imaging principle," Opt. Express **14**, 3887–3892 (2006).
12. C. C. Chiang, C. W. Tsai, and S. L. Tsao, "Design and simulation of a novel 32 × 32 photonic bandgap power switch based on SOI waveguide," Opt. Commun. **278**, 42–47 (2007).
13. M. F. Lu and Y. T. Huang, "Design of a photonic crystal taper coupler with different section lengths based on the multimode interference and the mode matching," Jpn. J. Appl. Phys. **47**, 1822–1827 (2008).
14. P. K. Wei and W. S. Wang, "A TE-TM mode splitter on lithium niobate using Ti, Ni, and MgO diffusions," IEEE Photon. Technol. Lett. **6**, 245–248 (1994).
15. Y. Ohtera, T. Sato, T. Kawashima, T. Tamamura, and S. Kawakami, "Photonic crystal polarization splitters," Electron. Lett. **35**, 1271–1272 (1999).
16. Y. Y. Li, M. Y. Li, P. F. Gu, Z. R. Zheng, and X. Liu, "Graded wavelike two-dimensional photonic crystal made of thin films," Appl. Opt. **47**, C70–C74 (2008).
17. D. Taillaert, H. Chong, P. I. Borel, L. H. Frandsen, R. M. De La Rue, and R. Baets, "A compact two-dimensional grating coupler used as a polarization splitter," IEEE Photon. Technol. Lett. **15**, 1249–1251 (2003).
18. D. R. Solli, C. F. McCormick, R. Y. Chiao, and J. M. Hickmann, "Photonic crystal polarizers and polarizing beam splitters," J. Appl. Phys. **93**, 9429–9431 (2003).
19. T. Liu, A. R. Zakharian, M. Fallahi, J. V. Moloney, and M. Mansuripur, "Design of a compact photonic-crystal-based polarizing beam splitter," IEEE Photon. Technol. Lett. **17**, 1435–1437 (2005).
20. C. Y. Guan, J. H. Shi, and L. B. Yuan, "Photonic crystal polarizing and non-polarizing beam splitters," Chin. Phys. Lett. **25**, 556–558 (2008).
21. Y. Morita, Y. Tsuji, and K. Hirayama, "Proposal for a compact resonant-coupling-type polarization splitter based on photonic crystal waveguide with absolute photonic bandgap," IEEE Photon. Technol. Lett. **20**, 93–95 (2008).
22. V. Zabelin, L. A. Dunbar, N. Le Thomas, R. Houdre, M. V. Kotlyar, L. O'Faolain, and T. F. Krauss, "Self-collimating photonic crystal polarization beam splitter," Opt. Lett. **32**, 530–532 (2007).
23. E. Schonbrun, Q. Wu, W. Park, T. Yamashita, and C. J. Summers, "Polarization beam splitter based on a photonic crystal heterostructure," Opt. Lett. **31**, 3104–3106 (2006).
24. V. Mocella, P. Dardano, L. Moretti, and I. Rendina, "A polarizing beam splitter using negative refraction of photonic crystals," Opt. Express **13**, 7699–7707 (2005).
25. R. Ulrich, "Light-propagation and imaging in planar optical waveguides," Nouv. Rev. Optique **6**, 253–262 (1975).
26. R. Ulrich and G. Ankele, "Self-imaging in homogeneous planar optical waveguides," Appl. Phys. Lett. **27**, 337–339 (1975).
27. D. C. Chang and E. F. Kuester, "A hybrid method for paraxial beam propagation in multimode optical waveguides," Trans. Microwave Theory Tech. **29**, 923–933 (1981).
28. N. Zhu, D. Dai, and S. He, "A hybrid modeling for the theoretical analysis of reflections in a multimode-interference coupler based on silicon-on-insulator nanowires," Opt. Commun. **281**, 3099–3104 (2008).
29. S. M. Liao, "Design and analysis of multimode interference-based photonic crystal polarizing beam splitter," thesis (National Chiao Tung University, 2008).